

The mass-function of primordial star clusters

Fernando Santoro and Peter A. Thomas ^{*}

Astronomy Centre, University of Sussex, Falmer, Brighton, BN1 9QJ

29 October 2018

ABSTRACT

We use the block model to generate merger trees for the first star clusters in a Λ CDM cosmology. Using a simple collapse model and cooling criterion, we determine which halos are able to form stars before being disrupted by mergers. We contrast the mass functions of all the resulting star clusters and those of primordial composition, i.e. star clusters that have not been contaminated by subclusters inside them. In confirmation of previous work, two generations of primordial star clusters are identified: low-temperature clusters that cool via molecular hydrogen, and high-temperature clusters that cool via electronic transitions. The former dominate by number, but the two populations contain a similar mass with the precise balance depending upon the details of the model. We speculate on the current-day distribution of Population-III stars.

Key words: galaxies: formation – galaxies: star clusters – stars: Population III

1 INTRODUCTION

In a Cold Dark Matter (CDM) cosmology, small structures are the first to collapse and these then cluster together in a hierarchical fashion, giving rise to the bottom-up picture of galaxy formation. In this paper, we use the term ‘primordial star cluster’ for the first objects that are able to cool and form, zero-metallicity, Population III stars. They are of interest both in their own right and because they may be responsible for reionization of the intergalactic medium.

In a primordial gas, whose main elements are hydrogen and helium and their derivatives, there are two main cooling mechanisms, dependent on the temperature: for halos with virial temperatures less than 8600 K the cooling is dominated by roto-vibrational excitations of hydrogen molecules, while those with higher temperatures cool mainly via electronic transitions.

In a landmark paper entitled “How small were the first cosmological objects?”, Tegmark et al. (1997, hereafter T97) analytically tracked a top-hat collapse to the point of virialization, at which point the gas was cooled at constant density. They accepted an object as having cooled if it met the criterion $T(0.75z_{\text{vir}}) \leq 0.75 T_{\text{vir}}$, where T_{vir} is the virial temperature and z_{vir} the virialization redshift. They found that the first generation of objects that cooled in a standard CDM scenario virialized at a redshift of 27 and had a baryonic mass of about $10^5 M_{\odot}$. In a later paper, Abel et al. (1998) redid the calculation with a different H_2 cooling func-

Table 1. Properties of the two generations of $3\text{-}\sigma$ halos to form in each of the cosmologies (from HSTC02): cosmological model; redshift at which the halo cools to 75 per cent of the virial temperature; virial temperature; total mass of the halo; baryonic mass of the halo.

| Model | $z_{0.75}$ | T_{vir}/K | M_{tot}/M_{\odot} | $M_{\text{bary}}/M_{\odot}$ |
|---------------|------------|---------------------------|----------------------------|-----------------------------|
| Generation 1 | | | | |
| SCDM | 19.5 | 3 600 | 1.6×10^6 | 1.2×10^5 |
| τ CDM | 10.8 | 4 500 | 5.0×10^6 | 9.2×10^5 |
| Λ CDM | 21.9 | 3 400 | 8.6×10^5 | 3.3×10^4 |
| Generation 2 | | | | |
| SCDM | 18.5 | 10 800 | 9.9×10^6 | 7.5×10^5 |
| τ CDM | 10.7 | 10 600 | 2.1×10^7 | 3.9×10^6 |
| Λ CDM | 20.6 | 10 400 | 5.7×10^6 | 2.2×10^5 |

tion and estimated a very similar virialization redshift but a smaller baryonic mass, $7 \times 10^3 M_{\odot}$.

In a paper somewhat cheekily entitled “How big were the first cosmological objects?”, (Hutchings et al. 2002, hereafter HSTC02) extended the previous work to include halos of higher mass. They found two distinct generations of halos: Generation 1 halos dominated by molecular cooling as in the previous work, and higher-mass, Generation 2 halos dominated by electronic cooling. The properties of these halos in three different versions of the CDM cosmology are listed in Table 1.

Note that the difference in cooling redshift between the two generations of halos is small (partly because the CDM fluctuation spectrum is flat on small scales and partly because cooling is more efficient in Generation 2 halos). This led HSTC02 to speculate that both generations of halos may

* E-mail: p.a.thomas@sussex.ac.uk

Table 2. Cosmological parameters: density parameter; cosmological constant in units of $\lambda_0 = \Lambda/3H_0^2$; current baryon density in units of the critical density; Hubble parameter in units of $h = H_0/100\text{km s}^{-1}\text{Mpc}^{-1}$; power spectrum shape parameter; root-mean-square dispersion of the density within spheres of radius $8h^{-1}\text{Mpc}$.

| Ω_0 | λ_0 | Ω_{b0} | h | Γ | σ_8 |
|------------|-------------|---------------|-----|----------|------------|
| 0.35 | 0.65 | 0.038 | 0.7 | 0.21 | 0.90 |

form Population III stars (whereas others have considered only the smaller, Generation 1 halos to be important).

There were two main deficiencies in the model of HSTC02. Firstly, they neglected substructure: the referee suggested that all Generation 2 halos will have Generation 1 halos inside them and so they will not be of primordial composition. We show below that primordial Generation 2 halos can exist. Secondly, they considered only $3\text{-}\sigma$ fluctuations. In reality there will be a gaussian distribution of overdensities leading to a wide range of halo masses virialising at any given redshift.

The present paper, as a continuation of the previous work, addresses these two points by using the Block Model of Cole & Kaiser (1988) to generate a merger history of collapsed halos. This allows us to follow a wide dynamic range of halo masses very efficiently. Within the merger tree, the properties of halos are calculated using the same chemical model as in HSTC02.

Our work complements that of other authors who are investigating first object formation using numerical simulations, e.g. Abel et al. (1998), Bromm, Coppi & Larson (1999), Abel, Bryan & Norman (2000), Fuller & Couchman (2000), Nakamura & Umemura (2001), Bromm, Coppi & Larson (2002) and Nakamura & Umemura (2002). They are able to follow the dynamical evolution of single star clusters in great detail, whereas we learn instead about the properties of the cluster population.

We describe our numerical method in Section 2. The properties of individual halos for a merger tree corresponding to an overdense region of the Universe are presented in Section 3 and the corresponding mass function is described in Section 4. Finally, Section 5 explores variations of the basic model and discusses the nature of the star clusters.

2 METHODOLOGY

In this paper, we use the popular ΛCDM cosmology whose parameters are tabulated in Section 2.1. The generation of a merger tree of collapsed halos is described in Section 2.2 and the criteria whereby we determine which of these form star clusters is outlined in Section 2.3.

2.1 Cosmology

HSTC02 investigated the cooling of halos in three different CDM cosmologies. In this paper, we restrict our attention to the currently-favoured ΛCDM cosmology whose parameters are listed in Table 2.

We have used the transfer function calculated by CMB-FAST. There have been recent suggestions that the normal-

isation of the power spectrum may be closer to 0.7 than 0.9 (e.g. Seljak 2002; Allen et al. 2002) this would have the effect of moving the formation epoch of the first star clusters to lower redshift and also lowering the amount of substructure.

2.2 Block Model

We generate a halo merger tree using the Block Model of Cole & Kaiser (1988). This starts with a ‘root’ block of mass M_0 and density fluctuation δ_0 . In this paper we fix $M_0 = 10^{11} M_\odot$ and choose two different values of δ_0 corresponding to a $3\text{-}\sigma$ fluctuation ($\delta_0 = 10.98$) and the mean density ($\delta_0 = 0$).

Geometrically the block can be visualised as a cuboid with sides in the ratio $1:2^{1/3}:2^{2/3}$, but the density fluctuations are calculated as for a spherical top-hat model of the same mass; given the uncertainty in the normalisation of the power spectrum, the distinction is of no importance. The block can be bisected by a plane perpendicular to its longest axis, creating two similar blocks of half the mass, $M_1 = M_0/2$. To generate density fluctuations in these daughter blocks, we add power drawn at random from a gaussian distribution with variance $\sigma^2(M_1) - \sigma^2(M_0)$; once again, this is an approximation, but a good one. A positive fluctuation is added to one block and an equal negative fluctuation to the other, so as to conserve the overall level of fluctuations in the root block.

The same procedure is then repeated, with each parent block being divided into two equal-mass daughters until the desired resolution is reached. In this paper, we use 21 levels, creating a total of $2^{21} - 1 \approx 2.1 \times 10^6$ blocks with a minimum block mass of $9.5 \times 10^4 M_\odot$.

We use a simple model in which the collapse of blocks to form bound objects is determined only by their overdensity. To be precise, we assume them to virialise once their linear overdensity reaches $\delta_c = 1.69$ (see Eke et al. 1996 and Lokas & Hoffman 2001 where only a very weak dependence on Ω has been found).

The equation for the rate of growth of δ with redshift, z , is

$$\delta(z) = \frac{\delta(0)}{1+z} \frac{g(\Omega)}{g(\Omega_0)}, \quad (1)$$

where

$$g(\Omega) = 2.5 \frac{\Omega}{\left(\frac{1}{70} + \frac{209}{140}\Omega - \frac{1}{140}\Omega^2 + \Omega^{\frac{4}{7}}\right)} \quad (2)$$

is the growth suppression factor (Viana & Liddle 1996) and

$$\Omega = \frac{\Omega_0}{\left(\Omega_0 + \left(\frac{1}{1+z}\right)^3 (1 - \Omega_0)\right)}. \quad (3)$$

In the binary tree generated by the Block Model, most of the blocks are contained in larger blocks of greater overdensity. Often this will be the immediate parent (one of the two daughters of each parent will have lesser density) but it could also be a block further up the tree. Under these circumstances, the larger block will collapse before the smaller, and so the latter will never attain an independent existence as a virialised structure. We eliminate these under-dense blocks from the tree and call the remaining blocks ‘halos’.

We have performed one hundred realizations of the

Block Model with different number seeds. We use these for both values of δ_0 as the set of halos is the same in each case. Unless stated otherwise, the results presented below are averages over all realizations.

2.3 Halo evolution and the formation of star clusters

We wish to know whether a halo can form stars before it gets incorporated into some larger structure. To do this, we construct an artificial model in which the halo has no sub-structure and cools at constant density. The actual structure of halos will be highly complex but our model gives a reasonable estimate of what is going on, short of doing a prohibitively time-consuming simulation.

We begin with the smallest halos and work our way up the merger tree. Each halo is treated as an isolated, isothermal sphere, as described in Section 3.3 of HSTC02. The mean baryon density within the virial radius, r_{vir} , is taken to be equal to

$$\rho_{\text{vir}} = \left(\frac{\Delta_c}{\Omega}\right) \rho_{b0}(1 + z_{\text{vir}})^3 \quad (4)$$

where z_{vir} is the virialization redshift, ρ_{b0} is the current mean density of baryons in the Universe, and Δ_c is the mean overdensity of the virialized halo in units of the critical density at that time, which we take to be $\Delta_c \approx 18\pi^2\Omega^{0.45}$ (Eke et al. 1998).

We define the dynamical time for each halo to be

$$t_{\text{dyn}} = \frac{1}{4\sqrt{2}} t_{\text{vir}} \quad (5)$$

where t_{vir} is the age of the universe at the time of virialization.

The virial temperature of the halo is

$$\begin{aligned} T_{\text{vir}} &= \frac{\mu m_H}{k_B} \frac{GM_{\text{tot}}}{2r_{\text{vir}}} \\ &\approx 40.8 \frac{\mu}{1.225} (1 + z_{\text{vir}}) \left(\frac{\Delta_c h^2 \Omega_0}{18\pi^2 \Omega}\right)^{\frac{1}{3}} \left(\frac{M_{\text{tot}}}{10^5 M_\odot}\right)^{\frac{2}{3}} \text{ K} \end{aligned} \quad (6)$$

Here M_{tot} is the total mass (dark plus baryonic), m_H is the mass of a hydrogen atom, k_B is the Boltzmann constant, G is the gravitational constant, and μ is the mean mass of particles in units of m_H . Note that equation (6) differs slightly from the equivalent expression in HSTC02 as the latter contains a typographical error.

The initial fractional abundance of molecular Hydrogen is taken to be 1.1×10^{-6} as calculated by Galli & Palla (1998), and the initial ionization fraction is taken to be the maximum of the equilibrium value at T_{vir} and the residual value from the early Universe, 1.33×10^{-4} .

Starting from these initial conditions, we determine the time that it would take the gas to cool isochorically to $T_{0.75} = 0.75 T_{\text{vir}}$, using the minimal model presented in Section 2 of HSTC02. This includes molecular hydrogen cooling, collisional excitation and ionization of hydrogen and helium, and inverse Compton cooling from cosmic microwave background photons.

If halos are unable to cool to $T_{0.75}$ before being swallowed by a more massive halo, then we assume that they are heated to the new virial temperature and that any sub-structure (which would be minimal anyway because of the

long cooling time) is erased. Contrarily, halos that can cool to $T_{0.75}$ are assumed to be able to (instantaneously) cool further to low temperatures and to form a star cluster.

For halos whose cooling times are much shorter than their dynamical times, then the gas will likely never get heated to the virial temperature in the first place and the assumption of instantaneous star formation will be a good one. However, for halos in which the cooling time exceeds the dynamical time then it seems likely that our model will underestimate the time taken to form stars. We consider in Section 5.2 the effect of adding a time-delay before star-formation and show that it favours the second generation of halos.

Star clusters may or may not survive subsequent halo mergers but either way they are assumed to instantly contaminate their surroundings with metals. Thus the primordial star clusters are those that contain no smaller star clusters within them. We assume that the metals do not propagate into halos on other branches of the tree. Thus metals may be ejected from star clusters but are confined within the next level of the merger hierarchy. This can be justified by a self-regulated model of star formation in which star-formation is terminated once gas is expelled from the star cluster.

We also assume that there is no external radiation field, other than that provided by the cosmic microwave background. Primordial star clusters will be surrounded by neutral gas and the propagation of ionizing photons will be severely limited. Nevertheless, these first objects will be highly clustered and so they will at some stage begin to interact with each other. We hope to consider this in a future paper.

3 HALO PROPERTIES

In this section, we present results for the overdense, 3- σ , root halo. A comparison with the mean-density root halo will be presented in Section 5.3.

3.1 Collapsed halos

We start by considering the properties of all collapsed halos, i.e. halos whose linear overdensity exceeds that of all the (more-massive) halos within which they are contained. In Figure 1 we plot the virialization redshift of such halos (drawn from all 100 realisations) against their virial temperature.

The banding comes about because the halos come in fixed masses. Thus the smallest halos of mass $9.5 \times 10^4 M_\odot$ correspond to the left-most band; they have a wide range of virialization redshifts and temperatures that vary between about 200 and 1200 K; the top-most point corresponds to a 6.2- σ and the lowest one to a 0.9- σ fluctuation. 20 other bands are then visible, one for each factor of two in mass until we reach the parent halo in the bottom-right which has a mass of $10^{11} M_\odot$, a virial temperature of $T_{\text{vir}} = 8.81 \times 10^5 \text{ K}$, and a virialization redshift of $z_{\text{vir}} = 7.1$ (corresponding to a 3- σ fluctuation on this scale). The bands are mostly parallel, except for the temperature range $T_{\text{vir}} \approx 10\,000\text{--}20\,000 \text{ K}$ within which the ionization level is changing.

The top panel of Figure 2 shows the cooling time, t_{cool} ,

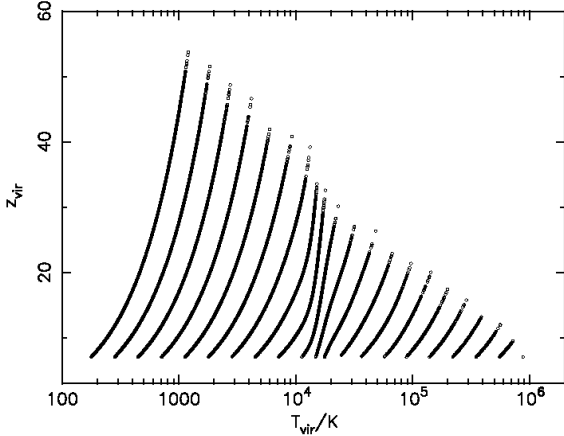


Figure 1. Virialization redshift, z_{vir} , versus virial temperature, T_{vir} , for all halos in the 100 realisations.

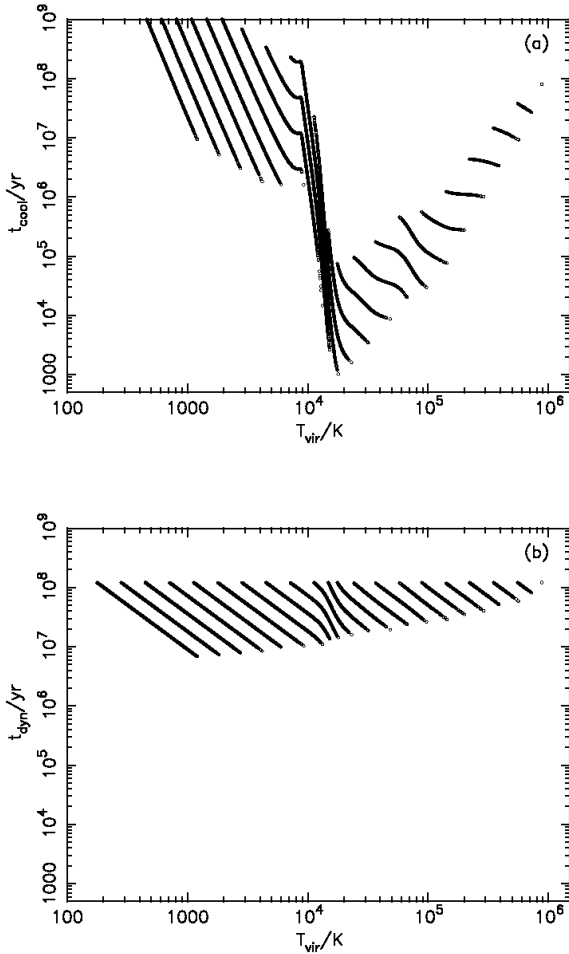


Figure 2. (a) The cooling time, t_{cool} , and (b) the dynamical time, t_{dyn} , for all collapsed halos, plotted against virial temperature.

versus the virial temperature for each of the halos shown in Figure 1. There is a sharp decline in the cooling time at $T_{\text{vir}} \approx 10\,000\text{ K}$ corresponding to the ionization temperature of hydrogen. Halos with higher virial temperatures than this (Generation 2 halos) are able to cool rapidly via electronic processes and so have relatively short cooling times. Those with lower virial temperatures (Generation 1) have to rely on cooling via molecular hydrogen which is formed only in very low quantities. Although our definition of t_{cool} only follows cooling down to $0.75 T_{\text{vir}}$, we note that Generation 2 halos have a high residual ionization at lower temperatures that acts as a catalyst to form molecular hydrogen: thus their cooling rates at low temperature are faster than for Generation 1 halos.

The lower panel of Figure 2 shows the dynamical time for the collapsed halos, as defined in equation 5. A rule of thumb, halos with virial temperatures above about $10\,000\text{ K}$ are able to cool in less than a dynamical time; cooler halos take longer.

3.2 Star clusters

The time difference, Δt_{coll} , between the collapse time of each halo and that of its parent is shown in the top panel of Figure 3. For a random location in space, one might expect that the time difference would be largest for massive, high-temperature halos. However, that is not the case for these realisations in which the top-level itself is constrained to collapse at $t = 0.69\text{ Gyr}$ (it is true for the halos considered in Section 5.3 for which the overdensity of the top-level halo is zero).

Those halos for which t_{cool} is less than Δt_{coll} can cool to a fraction 0.75 of their virial temperature before being swallowed up by their parent halo in the merger hierarchy. To begin with, we assume that this is a sufficient criterion to allow them to form stars and we identify them with star clusters. In reality the time-delay before star formation will be larger as the gas has to cool to low temperatures and to congregate into regions of high-density. We will consider the effect of allowing a longer time-delay in Section 5.2.

The lower panel in Figure 3 plots $\Delta t_{\text{coll}} - t_{\text{cool}}$ against the virial temperature. Those halos that lie above the line are those that form star clusters. Just 2 percent of all collapsed halos satisfy this condition. However, these are not distributed evenly over mass. For example, in the first three levels of the merger tree (i.e. the three levels with the lowest mass) only a fraction 1.2×10^{-7} , 8.4×10^{-5} and 3.2×10^{-3} of collapsed halos are able to form stars, whereas a successively higher fraction do so at higher mass. Only for the most massive halos with virial temperatures in excess of 10^5 K does the cooling time again begin to exceed the lifetime of halos.

3.3 Primordial star clusters

We assume that metal-enrichment from star-formation is instantaneous but that it does not extend beyond the immediate environment of a star cluster and its parent halo. Then star clusters of primordial composition are simply those which do not have any smaller star clusters contained within them.

Approximately half of these clusters (56.8%) in our $3\text{-}\sigma$ realisations satisfy this condition with the bias swinging

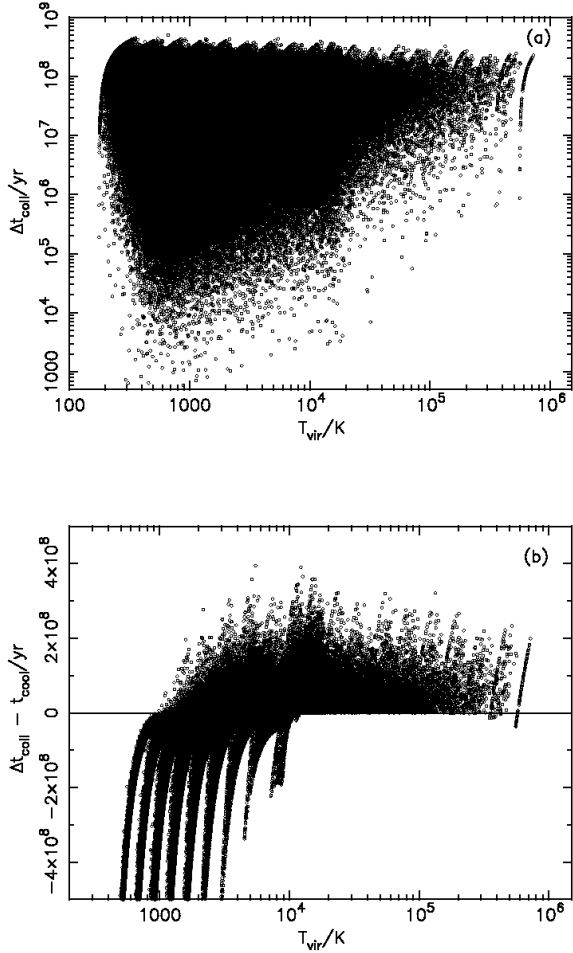


Figure 3. (a) The difference in collapse time of a halo and its parent, Δt_{coll} , and (b) the difference between the collapse time of a halo and its parent minus the cooling time of the halo, $\Delta t_{\text{coll}} - t_{\text{cool}}$, versus virial temperature. For clarity, the lower vertical axis in panel (b) has been truncated at -5×10^8 yr.

back towards low masses. The most massive primordial star cluster has a mass of $9.76 \times 10^7 M_{\odot}$ and a virial temperature of 1.54×10^4 K.

4 HALO MASS FUNCTIONS

The number of star clusters as a function of virial temperature, averaged over all 100 realisations, is shown in the upper panel of Figure 4. The upper histogram shows all star clusters, whereas the lower is restricted to primordial star clusters. There is a clear minimum at about 8600 K corresponding to the division between Generation 1 halos on the left and Generation 2 halos on the right. Note that the star clusters that make up the upper histogram are not all independent. That is to say that many of the low-temperature clusters are subcomponents of the higher-temperature ones. However, the primordial star clusters are all distinct objects. The y-scale in panel (a) could be multiplied by $3.94h^3 \text{Mpc}^{-3}$ to convert to a number density but we have not done this

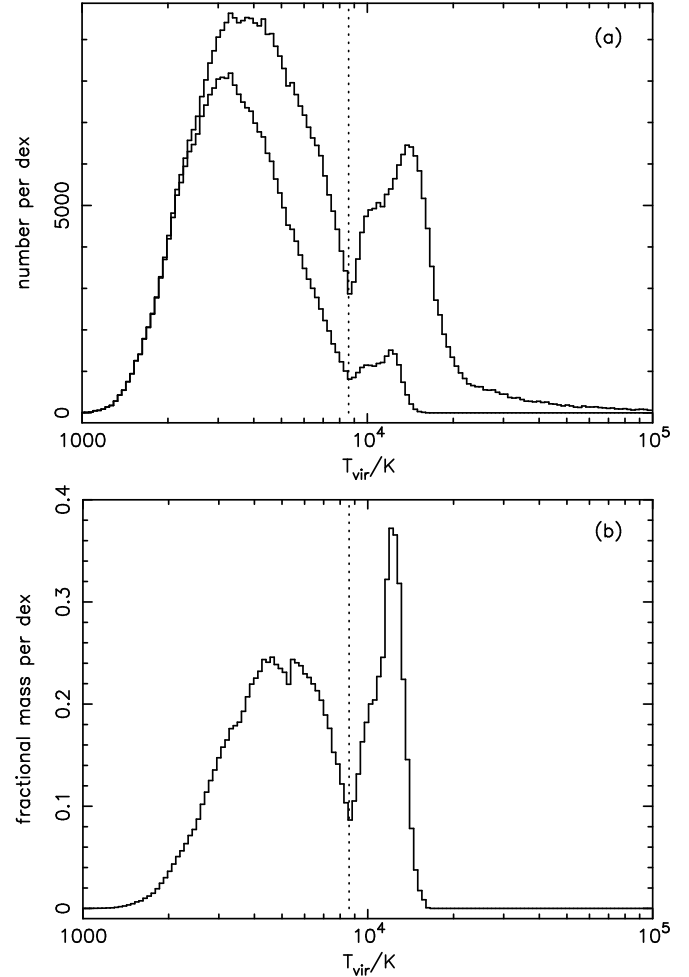


Figure 4. Histograms showing (a) the number of, and (b) the fractional mass contained in, star clusters as a function of their virial temperature. In panel (a) the upper line shows all star clusters whereas the low line is for clusters of primordial composition. Panel (b) shows only primordial halos. The minimum at $T_{\text{vir}} \approx 8600$ K is used to demarcate between the two generations of halos.

as the $3\text{-}\sigma$ region that we consider is not representative of all space.

The lower panel of Figure 4 shows the same distribution but weighted by mass. From this it is apparent that, whereas the majority of the primordial star clusters in this region are Generation 1 objects, the division of mass between the two generations is much more even, with only about twice as much mass contained in Generation 1 as compared to Generation 2 objects.

Note the sharp cut-off in the mass density of primordial star clusters at virial temperatures greater than about 15000 K. This is because all higher temperature clusters contain a Generation 2 subcluster for which the cooling time is very short and which can itself form stars on a short timescale. This situation changes when we introduce a time-delay for star formation in Section 5.2.

Figure 5 is similar to Figure 4 except that the ordinate is now virial mass rather than virial temperature (to convert to baryonic mass, the x-scale should be multiplied by 0.12). In panel (b), the dotted line shows the contribution to the total

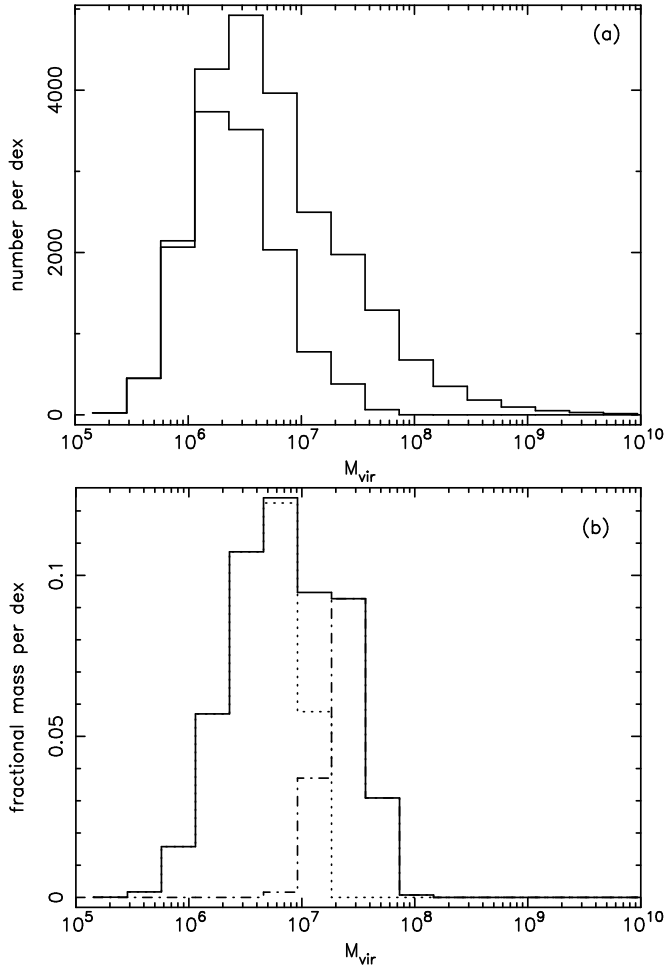


Figure 5. Histograms showing (a) the number, and (b) the mass fraction, of star clusters as a function of their virial mass. In panel (a) the upper line shows all star clusters whereas the low line is for clusters of primordial composition. Panel (b) shows only primordial clusters. The dotted line corresponds to Generation 1 halos ($T_{\text{vir}} < 8600$ K) and the dotted-dashed line correspond to Generation 2 halos.

mass of Generation 1 halos (whose virial temperature is less than 8600 K), while the dot-dashed line is for Generation 2 halos. The fractional mass contained in the two generations is 0.109 and 0.049, respectively. Thus about 16 per cent of all baryons in this $3\text{-}\sigma$ region of space will have at one time been part of a primordial star cluster.

Figure 6 contrasts the collapse and star-formation redshifts of both generations of halo. The spiky features visible in the distributions are due to the factor of two mass resolution of our halos and would be smoothed out in a more general merger tree. Because of the long cooling times of Generation 1 halos, the difference in the peaks of the distributions of star-formation redshifts of the two generations is not so great as for their collapse redshifts. Nevertheless, it is clear from the figure that a significant fraction of Generation 1 halos both collapse and form stars before Generation 2 halos begin to form in numbers. This highlights the need for a more sophisticated model of feedback than we attempt in this paper.

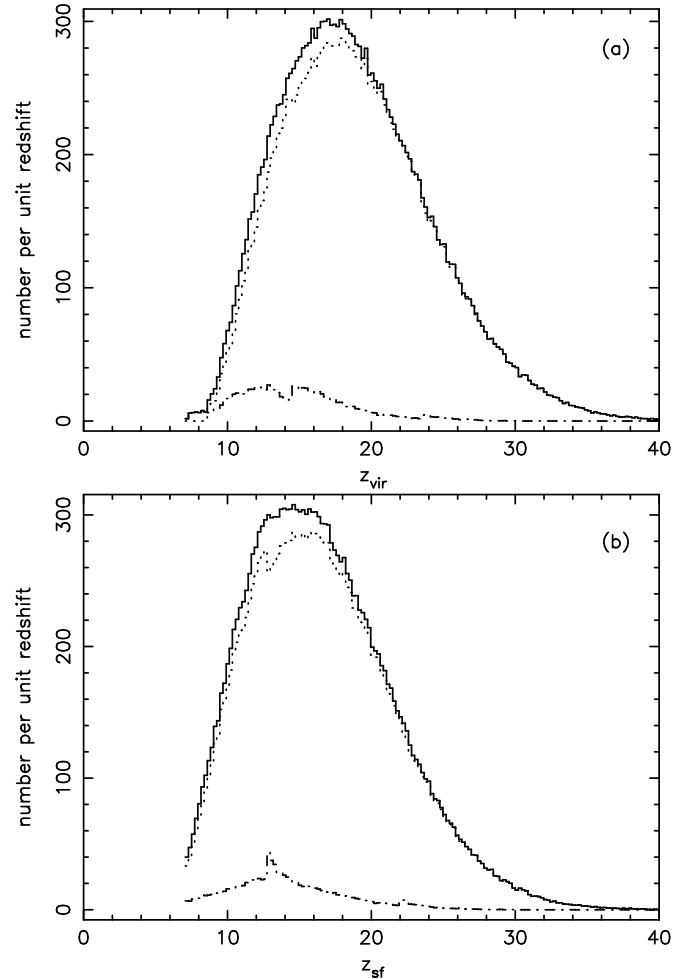


Figure 6. A histogram showing the number of primordial star clusters as a function of (a) their virialization redshift, and (b) their star-formation redshift. The dash-dotted and dotted lines correspond to Generation 1 and Generation 2 halos, respectively.

5 DISCUSSION

5.1 Numerical considerations

It is legitimate to ask to what extent our results are limited by the factor-of-two mass resolution inherent in the Block model. If we could have subhalos with a wider range of masses would that lead to a greater probability of contamination by star formation and a reduction in the fraction of primordial halos? The dramatic reduction in the cooling time of Generation 2 halos compared to their low-mass, Generation 1 subhalos, as illustrated by the upper panel in Figure 2, suggests that this is unlikely to be the case. We expect to move to a more realistic merger tree in future work.

Meanwhile, we have tested the sensitivity of our results to the precise choice of halos masses by performing a second hundred realizations of the merger tree with the root halo mass (and hence each level of the merger hierarchy) increased by a factor of $\sqrt{2}$, to $1.4 \times 10^{11} M_{\odot}$. Figure 7 shows the mass function of primordial halos for these simulations contrasted with our original simulation (dotted line). There is no significant difference between the two.

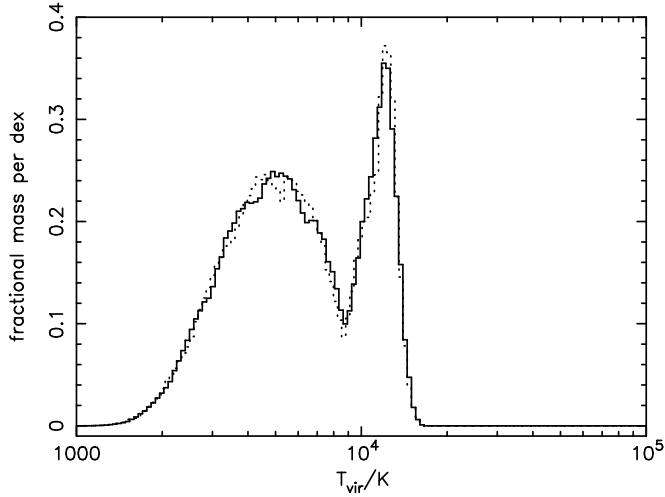


Figure 7. Histogram showing the mass fraction of primordial halos for two different choices of halo mass. The dotted line is the same as in Figure 4 (b) while the solid line shows the mass fraction for a merger tree in which the mass of the root halo has been increased a factor of $\sqrt{2}$.

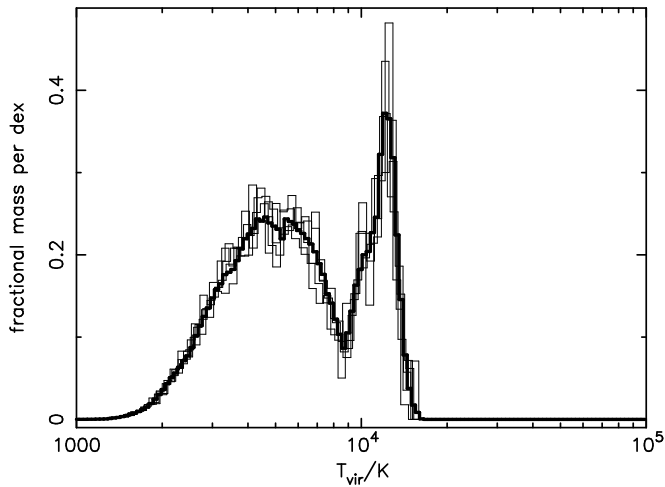


Figure 8. Histogram showing the effect of different realizations on the mass fraction of primordial objects as a function of virial temperature. The thick line corresponds to an average over 100 realizations.

The results that we have presented so far are an average over a large number of realisations. Figure 8 shows the dispersion around the average, of five of the 100 realisations carried out in this paper. It can be seen that the scatter is significant but not enough to seriously affect the divide between the two generations of star clusters within each realisation.

5.2 Time-delayed star-formation

So far we have assumed that after the cooling of the gas to low temperatures (following the T97 criterion) stars form instantaneously. In reality, there will be a lapse of time until the gas reaches the high-density regime in which nuclear reactions can take place and the stars are born. In an attempt to include in our code a time-delay between initial cooling

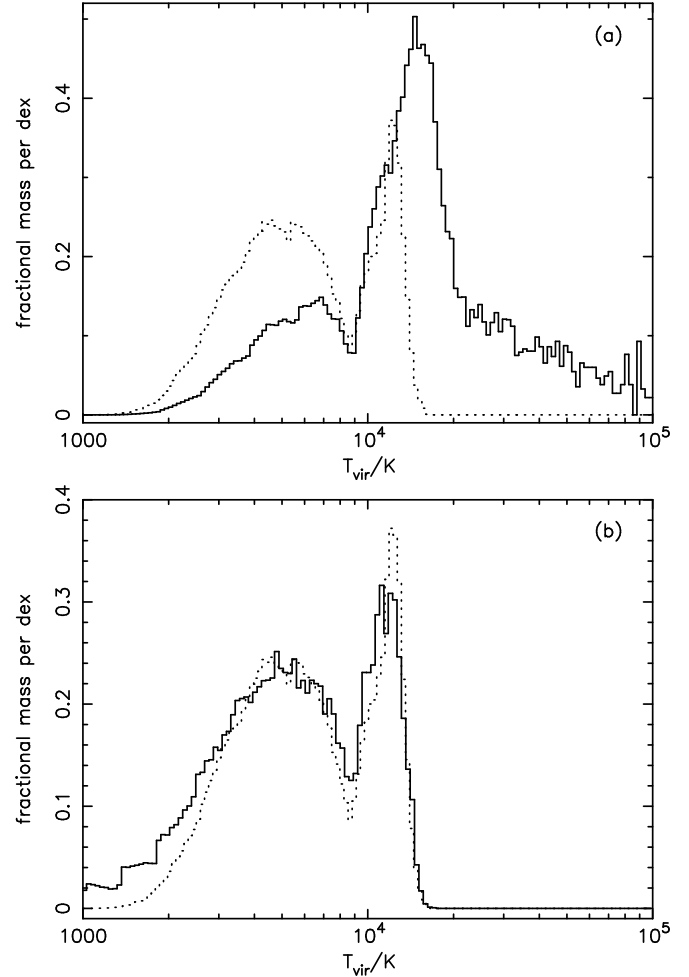


Figure 9. Histograms showing the mass fraction of primordial star clusters as a function of virial temperature. In Panel (a) the solid line shows the mass fraction of halos for which a dynamical time has been added to their cooling time. In Panel (b) the solid line shows the mass fraction for a zero-overdensity top-level merger tree. In both panels the dotted line is the same as in Figure 4 (b).

and star-formation, we consider in this section the effect of adding the dynamical time to the cooling time. The justification for this is simply that, following virialization, one would expect the gas to take at least a dynamical time to contract within the potential well of the halo (this argument has less force for high-mass halos whose cooling time is very much shorter than their dynamical time and which may therefore never attain virial equilibrium in the first place). Some evidence for this delayed star formation comes from Abel et al. (2002) who describe the formation of a primordial star using 3-D hydrodynamical simulation. Their results show that a cooled (~ 200 K) high redshift molecular cloud is formed at $z = 24$ and then a proto-star is formed at $z = 18.2$. The time that took to form this proto-star is of the order of the dynamical time of the cloud.

Panel (a) of Figure 9 shows a histogram of the fractional mass of primordial star clusters as a function of their virial temperatures. The dotted line corresponds to the original case in which no time delay has been added, while the full line shows the distribution when a dynamical time has

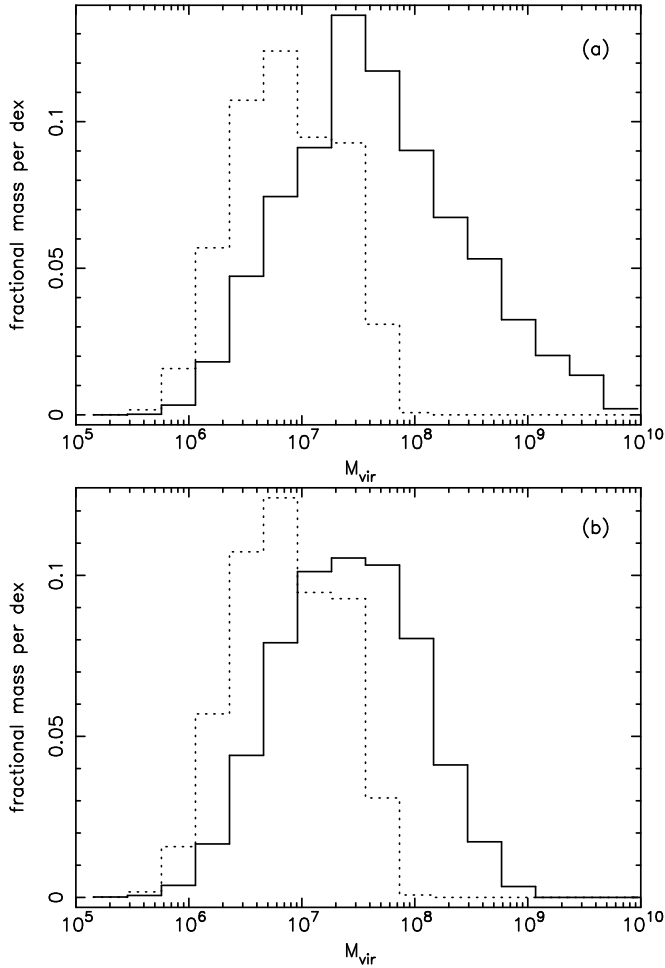


Figure 10. Histograms showing the mass fraction of primordial halos as a function of their virial mass. The dotted line in both panels is the same as in Figure 5 (b). In Panel (a) the solid line shows the mass fraction of halos for which a dynamical time has been added to their cooling time. In Panel (b) the solid line shows the mass fraction for a zero-overdensity top-level merger tree.

been added to their cooling time. The fractional mass has changed in such a way that now we have 3 times more mass in Generation 2 halos than in Generation 1 halos, and a greater total mass fraction than before. Note also that there is no longer a sharp cut-off at virial temperatures above 15 000 K because it is possible for subhalos to have short cooling times in this model and yet not to form stars.

Panel (a) in Figure 10 shows the equivalent mass function of these clusters from which it can be seen that halos as massive as $10^{10}M_{\odot}$ can contain primordial star clusters. While this does not seem very likely, the general conclusion that we draw is that delayed, rather than instantaneous, star-formation will favour Generation 2 halos over Generation 1.

We also tried a model with instantaneous star-formation but with a time-delay before energy and metallicity feedback. The idea is that if the time difference between the collapse of a parent halo and the cooling of its child is less than the time for the formation of supernovae, $\sim 10^7$ yr, then the parent halo will be of primordial composition and has to be added into the set of primordial objects. However,

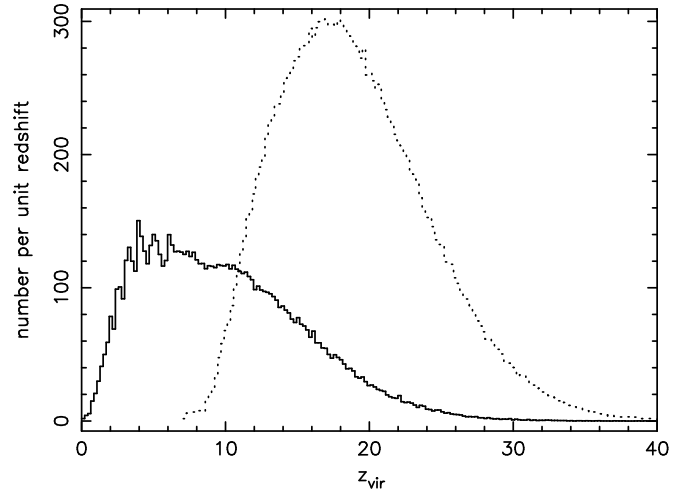


Figure 11. Histogram showing the distribution of collapse redshifts for primordial star clusters. The solid line is for a mean-density and the dotted line for the previously-investigated $3\text{-}\sigma$ regions.

this makes only a minor difference to our results and we will not discuss it further.

5.3 Mean-density regions

The first star clusters will form in overdense regions of the Universe, hence our use of a $3\text{-}\sigma$ root halo to this point. However, it is interesting to contrast these results with those expected for a more typical part of the Universe, with density equal to the cosmic mean.

Figure 11 contrasts the collapse redshifts of primordial star clusters for the $3\text{-}\sigma$ and mean density regions. It can be seen that the halos collapse at much lower redshifts in the mean overdensity case. Because the mean-density regions are likely to be far-removed from the regions of the first star-formation, they are unlikely to be affected by photoionizing photons at high redshift. However observations (e.g. Fan et al. 2002) and simulations (e.g. Razoumov et al. 2002) both suggest that the Universe became re-ionized at a redshift of about 6 and our model will be invalid after this time. This will mostly affect the evolution of Generation 2 halos.

The effect of the lower formation redshift on the virial temperatures and masses of the star clusters is shown in the lower panels of Figures 9 and 10. The fractional mass distribution over virial temperature is almost unchanged, but with a slight bias towards lower temperatures compared with the $3\text{-}\sigma$ case. A greater effect is a shift in the mass function towards higher masses: because the halos collapse at lower redshift and hence have lower densities, they have higher masses for a given virial temperature.

5.4 What and where are they now?

Our model predicts the masses, virial temperatures and formation redshifts of primordial star clusters, but says nothing about their internal structure. Hydrodynamical simulations (see references in the Introduction) have made a start in this direction but are as yet still in their infancy. There has been some theoretical speculation about the masses of the first

stars but no consensus has emerged. In this section, we use our results to discuss two possible fates of primordial star clusters, but note that the physics is sufficiently uncertain that we may even have got the roles of the two generations mixed up.

The baryonic mass of our root halos, $1.2 \times 10^{10} M_{\odot}$, is similar to that of a normal galaxy of mass approximately one-tenth that of an L_* galaxy. The space-density for the 3-sigma fluctuations on this scale is $3.0 \times 10^3 h^3 \text{Mpc}^{-3}$, similar to that of groups of galaxies, so that we would perhaps expect one such galaxy in a typical group. The other galaxies will form slightly later and so the star clusters will be biased to higher masses, although the total mass contained in primordial star clusters will be similar (see Section 5.3). Our model therefore suggests that approximately one tenth of the baryons in a typical galaxy will have passed through a primordial star cluster. The majority of these are probably enriched with processed material without themselves forming a zero-metallicity star.

The majority of Population III stars will be born in regions that are destined to end up in normal galaxies. However, our model does not preclude the formation of some zero-metallicity stars in low-density regions of the Universe at relatively low redshift (but before re-ionization). The resulting star clusters would be of low-density and therefore very hard to detect.

The bulk of Generation 1 star clusters at high redshift have masses in the range 10^6 – $10^7 M_{\odot}$; the baryonic mass is lower, 10^5 – $10^6 M_{\odot}$. It is natural, therefore, to identify these objects with the low-metallicity globular clusters found in the bulges and halos of normal galaxies. The relatively long cooling times of Generation 1 halos compared to their dynamical times would have aided dissipative collapse within the dark matter halo and survivability of the star cluster. One objection to this is that zero-metallicity stars have not been discovered in globulars, but of course the first stars may have been of high mass and may have burnt out long ago. A more serious objection is that we know that the amount of material in globular clusters is much less than one tenth of all the baryons in a galaxy. It is therefore probable that feedback of energy from the first supernovae (or hypernovae) will disrupt the star clusters and that the majority of zero-metallicity stars, should they still exist, will be spread throughout the bulges of normal galaxies.

The main differences with Generation 2 clusters is that they are more massive by about a factor of ten and that their cooling times are much shorter. It is interesting to speculate that electronic cooling when it did turn on would lead to catastrophic accumulation of cold gas at the centre of the collapsing halo and perhaps to the formation of a massive black hole. Observations (e.g. Ferrarese & Merritt 2000; Gebhardt et al. 2000) give a galactic black-hole to bulge mass ratio of about 0.001. To be consistent with this would require an accretion efficiency of just 2 per cent, creating seed holes of mass 2×10^4 – $2 \times 10^5 M_{\odot}$. Subsequent merging of these seed holes could lead to the formation of supermassive black holes in the centres of normal galaxies today.

ACKNOWLEDGEMENTS

FS thanks his parents for their support; PAT is a PPARC Lecturer Fellow.

REFERENCES

- Abel T., Anninos P., Norman M. L., Zhang Y., 1998, *ApJ*, 508, 518
 Abel T., Bryan G. L., Norman M. L., 2000, *ApJ*, 540, 39
 Abel T., Bryan G. L., Norman M. L., 2002, *Science*, 295, 93
 Allen S. W., Schmidt R. W., Fabian A., Ebeling H., 2002, Cosmological constraints from the local X-ray luminosity function of the most X-ray luminous galaxy clusters, *MNRAS*, submitted (astro-ph/0208394)
 Bromm V., Coppi P. S., Larson R. B., 1999, *ApJ*, 527, L5
 Bromm V., Coppi P. S., Larson R. B., 2002, *ApJ*, 564, 23
 Cole S., Kaiser N., 1988, *MNRAS*, 233, 637
 Eke V. R., Cole S., Frenk C. S., 1996, *MNRAS*, 282, 263
 Eke V. R., Navarro J. F., Frenk C. S., 1998, *ApJ*, 503, 569
 Fan X., Narayanan V. K., Strauss M. A., White R. L., Becker R. H., Pentericci L., Rix H., 2002, *AJ*, 123, 1247
 Ferrarese L., Merritt D., 2000, *ApJ*, 539, L9
 Fuller T. M., Couchman H. M. P., 2000, *ApJ*, 544, 6
 Galli D., Palla F., 1998, *AAP*, 335, 403
 Gebhardt K., Bender R., Bower G., Dressler A., Faber S. M., Filippenko A. V., Green R., Grillmair C., Ho L. C., Kormendy J., Lauer T. R., Magorrian J., Pinkney J., Richstone D., Tremaine S., 2000, *ApJ*, 539, L13
 Hutchings R. M., Santoro F., Thomas P. A., Couchman H. M. P., 2002, *MNRAS*, 330, 927
 Lokas E. L., Hoffman Y., 2001, in Identification of Dark Matter. The spherical collapse model in a universe with cosmological constant. p. 121
 Nakamura F., Umemura M., 2001, *ApJ*, 548, 19
 Nakamura F., Umemura M., 2002, *ApJ*, 569, 549
 Razoumov A. O., Norman M. L., Abel T., Scott D., 2002, *ApJ*, 572, 695
 Seljak U., 2002, submitted to *MNRAS*, astro-ph/0111362
 Tegmark M., Silk J., Rees M. J., Blanchard A., Abel T., Palla F., 1997, *APJ*, 474, 1
 Viana P. T. P., Liddle A. R., 1996, *MNRAS*, 281, 323